Coupled Electro-Thermal Transients Simulation of Gas-Insulated Transmission Lines Using FDTD and VEM Modeling

D. I. Doukas, T. A. Papadopoulos, A. I. Chrysochos, D. P. Labridis and G. K. Papagiannis

***Abstract*—In this paper, detailed mathematical formulation considering a coupled electro-thermal model for transient studies on transmission systems is presented. Regarding the thermal modeling, volume-element-method (VEM) is used to represent heat transfer equations on a 2D axisymmetric line model to be solved and temperature distribution over space and time to be determined. For the modeling of the electric part, a constant-parameter (CP) finite-difference time-domain (FDTD) method is utilized to calculate voltages and currents over space and time. The analysis is conducted on a gas-insulated transmission line (GIL) to highlight the electric and thermal domain interaction in case of transients. A set of fault scenarios are imposed on the electric part and transient analysis is conducted while considering the line thermal performance.**

***Index Terms*—coupled electro-thermal modeling, finite-difference time-domain (FDTD), gas-insulated transmission line (GIL), short-circuits, transients, volume-element-method (VEM).**

I. Introduction

GIL were first proposed as an alternative transmission system in Japan and due to their specific characteristics described in [1], they are preferred in case of high-capacity but short-distance links. A characteristic example of such an installation is the 275 kV-3.3 km Shinmeika-Tokai project described in [2]. Main advantages of GILs are the low electrical losses, the increased safety and operation aspects, such as limited need for reactive compensation and non-aging characteristic of gases [3]. The possibility of installing GILs in structures along with application issues to be addressed by necessary studies is discussed in [4].

Several studies have addressed a series of issues considering GIL operation. Heat transfer characteristics of GILs under varying temperature conditions were studied in [5], while coupled electromagnetic and thermal problems in GILs were discussed in [6]. Finally, [7]–[10] focused on technical aspects, such as insulation co-ordination, magnetic fields and modeling.

Moreover, transient simulation techniques and corresponding computational tools are becoming increasingly relevant to the design and analysis of transmission systems, such as GILs. Reliable tools are useful to provide a framework of secure operation and identify limitations, difficult to test even through experimental setups. Most modeling methodologies focus on the electromagnetic analysis of power systems, mainly for operating and optimization purposes in order to simulate their performance under different conditions, geometries and material properties. Additionally, thermal analysis is crucial, since it is vital to keep operating conditions within certain limits and prevent further equipment damage.

The scope of this paper is to present an efficient methodology in the area of coupled electro-thermal modeling for GIL by combining discretization techniques such as VEM methodology for the thermal part and FDTD for the electric part, respectively. The flexible parabolic-elliptic partial differential equations (PDEPE) solver [11] of MATLAB® [12] is used to calculate the temperature profile for all GIL layers over varying time and space. Heat transfer by conduction, convection and radiation is considered, and the analysis is applied on the GIL configuration presented in [1].

The contribution of this paper is to extend similar models developed only for the thermal analysis in terms of solver efficiency and to provide a fully analytic coupled electro-thermal model of GIL. This paper proposes a generic and accurate model that can be used as an efficient simulation and design tool to analyze any GIL. The proposed model predicts thermal behavior for transient conditions and can be useful to identify an overall framework of secure operation.

In Sections II and III the thermal problem formulation and the VEM analysis are presented, respectively. In Section IV the FDTD formulation for the electric modeling part is presented, whereas in Section V the electro-thermal coupling is described. Section VI is devoted to results and finally Section VII concludes the paper.

II. Thermal Problem Formulation

Thermodynamics and heat transfer laws are expressed by partial differential equations (PDEs) written in the generic form of (1). PDEs are introduced into PDEPE solver of MATLAB®, which deals with initial-boundary value problems for varying space z and time t.

$$c\left(z,t,T,\frac{\partial T}{\partial z}\right)\frac{\partial T}{\partial t} = z^{-m}\frac{\partial}{\partial z}\left[z^m f\left(z,t,T,\frac{\partial T}{\partial z}\right)\right] + s\left(z,t,T,\frac{\partial T}{\partial z}\right). \quad (1)$$

D. I. Doukas, A. I. Chrysochos, D. P. Labridis and G. K. Papagiannis are with the School of Electrical and Computer Engineering, Aristotle University of Thessaloniki, 54124 Thessaloniki, Greece (e-mail: doux@auth.gr).

T. A. Papadopoulos is with the Power Systems Laboratory, Department of Electrical and Computer Engineering, Democritus University of Thrace, 67100 Xanthi, Greece (e-mail: thpapad@ee.duth.gr).

Paper submitted to the International Conference on Power Systems Transients (IPST2017) in Seoul, Republic of Korea June 26-29, 2017.

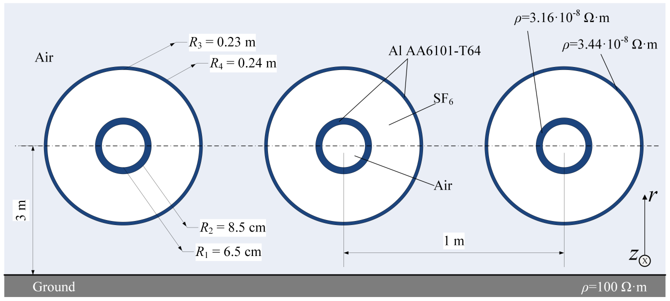

Fig. 1. GIL configuration.

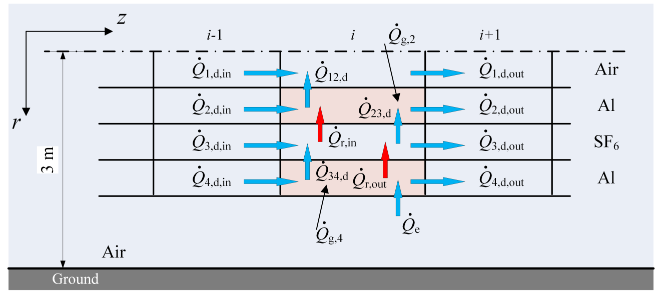

Fig. 2. Heat transfer and volume element discretization.

All PDEs hold for $t_0 \leq t \leq t_f$ and $a \leq z \leq b$, where t_0 and t_f represent the start and end time of simulation, while a and b represent the sending and receiving end of the GIL. Superscript m corresponds to the symmetry and can be 0, 1 or 2 for slab, cylindrical or spherical symmetry, respectively. Considering the numerical solution of (1), it is important to define the vector functions of flux $f(z, t, T, \frac{\partial T}{\partial z})$ and source $s(z, t, T, \frac{\partial T}{\partial z})$ terms. The coupling of the partial derivatives with respect to time is restricted by multiplying with a diagonal matrix $c(z, t, T, \frac{\partial T}{\partial z})$, with diagonal elements either zero for elliptic equations or positive for parabolic equations [11].

Initial conditions for the simulation start $t = t_0$ and all z, i.e., over the whole length, are given by:

$$T(z, t_0) = T_0(z). \tag{2}$$

Boundary conditions for all t and for one of the GIL terminations, a or b, are determined by (3) and are expressed in terms of the flux term f. Therefore, two boundary conditions are introduced for the whole timespan, one for $z = a$ and one for $z = b$. Vector functions p and q are both time and space dependent, whereas only p may depend also on T. The elements of q are either identically zero or never zero.

$$p(z, t, T) + q(z, t) f\left(z, t, T, \frac{\partial T}{\partial z}\right) = 0. \tag{3}$$

Scalars z and t are considered as inputs, while vectors T and $\frac{\partial T}{\partial z}$ represent the solution T and its partial derivative with respect to z, respectively. The solution T for the thermal problem is the temperature distribution for varying space and time. PDEPE calculates temperature distribution over space and time for all finite volume elements (VEs) of any layer. As initial conditions in this work, temperature at $t = t_0$ and all z for GIL layers is considered.

III. VEM Analysis

VEM analysis divides GIL layers in finite volumes using cylindrical coordinates for simultaneous discretization over time and space. Energy equations in terms of thermodynamics and heat transfer are solved in order to identify the variation of properties, such as temperature, over the GIL length and time. The analysis that follows results in a system of PDEs representing heat transfer, between VEs in r and z directions.

TABLE I
Material Properties and Initial Conditions

Material	k (W/mK)	ρ (kg/m^3)	c_v (J/kgK)	T_{init} (°C)
Aluminum	226	2700	895	27
SF_6	0.0136	6.2	56.928	27
Air	0.0257	1.225	718	27

The GIL geometry studied in this paper is based on [1], for long-distance GILs. The configuration is illustrated in Fig. 1. All relative permeabilities are equal to 1.0, while the conductor and enclosure permittivity is 1.057 and 1.0, respectively.

The mathematical formulation can be easily extended and applied to any cross-section regardless complexity. Such formulation is typically used in complex configurations where either gases [13] or liquids, as for example in case of liquid nitrogen-cooled superconducting cables are used [14]. Aluminum A1 AA 6101-T64 is considered as the conducting material for both the GIL conductor and enclosure, while sulfur hexafluoride SF_6 is used for insulation. For the inner pipe air is considered. Details on the material properties and the initial conditions T_{init} are given in Table I. Temperature conditions are within limits provided by IEEE in [15], [16].

Although in this configuration only heat transfer by conduction and radiation will be considered, expressions describing heat transfer by convection can be also incorporated. In Fig. 2 heat transfer reference directions are represented by arrows between consecutive volumes on both r and z directions. For brevity, discretization for only one of the GIL units is presented in Fig. 2 whereas the same analysis is applied on the other two units as well. The discretization approach as shown in Fig. 2 as well as the heat transfer model expressed by (4)–(10) are based in the analysis of [13], [14]. Note that the flux term f of (1) represents heat transfer on z direction, while the source term s the respective heat transfer on r direction.

A. Conduction

Between two consecutive VEs of solid materials heat transfer by conduction on both radial and axial directions takes place. Heat transfer by conduction is represented in Fig. 2 by blue color arrows. The expressions for heat conduction in $i-1$, i and $i+1$ consecutive VEs of the l^{th} layer, all consisting of the same material with thermal conductivity k_l, of a cross-section $A_{r,l}$ on z direction are given by:

$$\begin{cases} \dot{Q}^i_{l,\mathrm{d,in}} = -\frac{k_l A_{r,l}(T^i_l - T^{i-1}_l)}{\Delta_z^{i-1}} \\ \dot{Q}^i_{l,\mathrm{d,out}} = -\frac{k_l A_{r,l}(T^{i+1}_l - T^i_l)}{\Delta_z^{i+1}}. \end{cases} \tag{4}$$

Similarly, the expressions for heat conduction for consecutive VEs of the i^{th} cross-section of the GIL between different l_1 and l_2 GIL layers, on r direction are given by

$$\dot{Q}^i_{l_1 l_2,\mathrm{d}} = U^i_{l_1 l_2}(T^i_{l_2} - T^i_{l_1}) \tag{5}$$

where $U^i_{l_1 l_2}$ is

$$U^i_{l_1 l_2} = \left(\frac{\ln \frac{2R_{l_1}}{R_{l_1-1}+R_{l_1}}}{2\pi k_{l_1} \Delta^i_z} + \frac{\ln \frac{R_{l_1}+R_{l_2}}{2R_{l_1}}}{2\pi k_{l_2} \Delta^i_z} \right)^{-1} \tag{6}$$

where R_{l_1}, R_{l_2} and R_{l_1-1} are the radii of layers l_1, l_2 and of the inner layer before l_1, respectively. Equation (5) is also used to calculate $\dot{Q}_{\mathrm{e}}$, which is the amount of heat exchange by conduction from the environment.

B. Convection

Heat transfer by convection might exist also both on the r and z directions between different solid and liquid materials. For mass flow $\dot{m}_l$ and specific heat c_{p_l}, heat convection for consecutive VEs on z and r directions is given by

$$\begin{cases} \dot{Q}^i_{l,\mathrm{v,in}} = -\dot{m}_l c_{p_l}(T^i_l - T^{i-1}_l) \\ \dot{Q}^i_{l,\mathrm{v,out}} = -\dot{m}_l c_{p_l}(T^{i+1}_l - T^i_l) \end{cases} \tag{7}$$

$$\dot{Q}^i_{l_1 l_2,\mathrm{v}} = h_{l_1} A^i_{l_1,l_2}(T^i_{l_2} - T^i_{l_1}) \tag{8}$$

where for Nusselt number Nu and hydraulic diameter D_h, h_{l_1} equals

$$h_{l_1} = \frac{k_{l_1}\mathrm{Nu}}{D_h}. \tag{9}$$

C. Radiation

Heat radiation occurs between the GIL conductor and the outer enclosure, as seen in Fig. 2 with red arrows, where SF_6 is imposed. Given that A^i_l correspond for the cylindrical surfaces and not the cross-sections, heat radiation for consecutive VEs of the i^{th} line cross-section between different l_1 and l_2 GIL layers, that surround SF_6 layer, on r direction is given by

$$\begin{cases} \dot{Q}^i_{\mathrm{r,in}} = -\frac{\varepsilon_{l_1}}{1-\varepsilon_{l_1}} A^i_{l_1}\left[B_1 - \sigma(T^i_{l_1})^4\right] \\ \dot{Q}^i_{\mathrm{r,out}} = -\frac{\varepsilon_{l_2}}{1-\varepsilon_{l_2}} A^i_{l_2}\left[\sigma(T^i_{l_2})^4 - B_2\right] \end{cases} \tag{10}$$

where σ is the Stefan-Boltzmann constant, ε is the material emissivity and B_1 and B_2 are determined in [13].

D. GIL Modeling

For the GIL cross-section and the heat transfer representation illustrated in Figs. 1 and 2, respectively, PDEs that represent the application of the first law of thermodynamics are derived for the i^{th} VE of all layers. Since each GIL unit consists of 4 layers, 4 PDEs are presented. All PDEs are expressed in the form of (1), in which on the left side of the equation is the coupling term c, whereas on the right side the flux f and source s terms, respectively. Heat transfer on the z axis, i.e., $\dot{Q}^i_{l,\mathrm{d,in}}$ and $\dot{Q}^i_{l,\mathrm{d,out}}$ represent the flux term f. Heat transfer on the r axis, i.e., $\dot{Q}^i_{l_1 l_2,\mathrm{d}}$, $\dot{Q}^i_{\mathrm{r,in}}$, $\dot{Q}^i_{\mathrm{r,out}}$ and $\dot{Q}_{\mathrm{e}}$ represent the source term s. Heat generation on conductors, expressed as $\dot{Q}_{\mathrm{g},l}$, is also part of the source term s. The temperature distribution over space and time is represented in (11)–(14). Although (11)–(14) refer to only one of the GIL units, the same formulation applies for the remaining ones. GIL units are considered thermally isolated with each other.

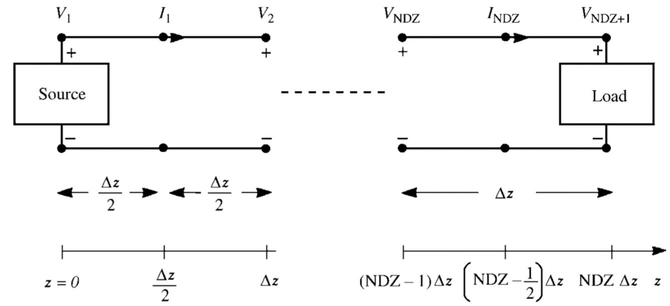

Fig. 3. Line discretization into NDZ segments for the FDTD analysis [17].

$$\underbrace{\left(c_{v_{\mathrm{Air}}}\rho_{\mathrm{Air}}A_{r,1}\Delta^i_z\right)}_{\text{coupling } c}\frac{\partial T^i_1}{\partial t} = \underbrace{\dot{Q}^i_{1,\mathrm{d,in}} - \dot{Q}^i_{1,\mathrm{d,out}}}_{\text{flux } f} + \underbrace{\dot{Q}_{12,\mathrm{d}}}_{\text{source } s} \tag{11}$$

$$\begin{aligned} \left(c_{v_{\mathrm{Al}}}\rho_{\mathrm{Al}}A_{r,2}\Delta^i_z\right)\frac{\partial T^i_2}{\partial t} &= \dot{Q}^i_{2,\mathrm{d,in}} - \dot{Q}^i_{2,\mathrm{d,out}} \\ &\quad - \dot{Q}_{12,\mathrm{d}} + \dot{Q}_{23,\mathrm{d}} + \dot{Q}_{\mathrm{r,in}} + \dot{Q}^i_{\mathrm{g},2} \end{aligned} \tag{12}$$

$$\begin{aligned} \left(c_{v_{\mathrm{SF}_6}}\rho_{\mathrm{SF}_6}A_{r,3}\Delta^i_z\right)\frac{\partial T^i_3}{\partial t} &= \dot{Q}^i_{3,\mathrm{d,in}} - \dot{Q}^i_{3,\mathrm{d,out}} \\ &\quad - \dot{Q}_{23,\mathrm{d}} + \dot{Q}_{34,\mathrm{d}} \end{aligned} \tag{13}$$

$$\begin{aligned} \left(c_{v_{\mathrm{Al}}}\rho_{\mathrm{Al}}A_{r,4}\Delta^i_z\right)\frac{\partial T^i_4}{\partial t} &= \dot{Q}^i_{4,\mathrm{d,in}} - \dot{Q}^i_{4,\mathrm{d,out}} \\ &\quad - \dot{Q}_{34,\mathrm{d}} + \dot{Q}_{\mathrm{e}} - \dot{Q}_{\mathrm{r,out}} + \dot{Q}^i_{\mathrm{g},4} \end{aligned} \tag{14}$$

IV. FDTD Formulation

For the FDTD modeling, the formulation methodology of lossy multiconductor transmission lines, of [17], is used, as seen in Fig. 3. CP FDTD is used to reduce simulation time.

First, the voltages along the line are calculated, for a fixed timestep Δt and n time instants, in terms of the past solutions.

$$\begin{aligned} \mathbf{V}^{n+1}_k &= \left(\frac{\Delta z}{\Delta t}\mathbf{C} + \frac{\Delta z}{2}\mathbf{G}\right)^{-1}\left(\frac{\Delta z}{\Delta t}\mathbf{C} - \frac{\Delta z}{2}\mathbf{G}\right)\mathbf{V}^n_k \\ &\quad - \left(\frac{\Delta z}{\Delta t}\mathbf{C} + \frac{\Delta z}{2}\mathbf{G}\right)^{-1}\left(\mathbf{I}^{n+1/2}_k - \mathbf{I}^{n+1/2}_{k-1}\right) \end{aligned} \tag{15}$$

, for $k = 2, 3, ...\mathrm{NDZ}$.

Next currents are calculated by means of the calculated voltages and past current values. The solution starts with an initially relaxed line having zero voltage and current values.

$$\mathbf{I}_k^{n+3/2} = \left(\frac{\Delta z}{\Delta t}\mathbf{L} + \frac{\Delta z}{2}\mathbf{R}\right)^{-1}\left(\frac{\Delta z}{\Delta t}\mathbf{L} - \frac{\Delta z}{2}\mathbf{R}\right)\mathbf{I}_k^{n+1/2} - \left(\frac{\Delta z}{\Delta t}\mathbf{L} + \frac{\Delta z}{2}\mathbf{R}\right)^{-1}\left(\mathbf{V}_{k+1}^{n+1} - \mathbf{V}_k^{n+1}\right) \quad (16)$$

, for $k = 1, 2, ...\mathrm{NDZ}$.

Finally, incorporation of the terminal conditions is considered. The essential problem in incorporating the terminal conditions in FDTD is that voltages and currents at each end of the line, V_1, I_1 and $V_{\mathrm{NDZ}+1}$, I_{NDZ}, are not collocated in space or time, whereas the terminal conditions relate the voltage and current at the same position and at the same time.

$$\mathbf{V}_1^{n+1} = \left(\frac{\Delta z}{\Delta t}\mathbf{R}_{\mathrm{S}}\mathbf{C} + \frac{\Delta z}{2}\mathbf{R}_{\mathrm{S}}\mathbf{G} + \mathbf{1}_n\right)^{-1}\left[\left(\frac{\Delta z}{\Delta t}\mathbf{R}_{\mathrm{S}}\mathbf{C} - \frac{\Delta z}{2}\mathbf{R}_{\mathrm{S}}\mathbf{G} - \mathbf{1}_n\right)\mathbf{V}_1^n - 2\mathbf{R}_{\mathrm{S}}\mathbf{I}_1^{n+1/2} + \left(\mathbf{V}_{\mathrm{S}}^{n+1} - \mathbf{V}_{\mathrm{S}}^n\right)\right] \quad (17)$$

$$\mathbf{V}_{\mathrm{NDZ}+1}^{n+1} = \left(\frac{\Delta z}{\Delta t}\mathbf{R}_{\mathrm{L}}\mathbf{C} + \frac{\Delta z}{2}\mathbf{R}_{\mathrm{L}}\mathbf{G} + \mathbf{1}_n\right)^{-1}\left[\left(\frac{\Delta z}{\Delta t}\mathbf{R}_{\mathrm{L}}\mathbf{C} - \frac{\Delta z}{2}\mathbf{R}_{\mathrm{L}}\mathbf{G} - \mathbf{1}_n\right)\mathbf{V}_{\mathrm{NDZ}+1}^n + 2\mathbf{R}_{\mathrm{L}}\mathbf{I}_{\mathrm{NDZ}}^{n+1/2} + \left(\mathbf{V}_{\mathrm{L}}^{n+1} - \mathbf{V}_{\mathrm{L}}^n\right)\right] \quad (18)$$

$\mathbf{C}$, $\mathbf{G}$, $\mathbf{L}$ and $\mathbf{R}$ are 6×6 matrices that have derived from the calculation of the per-unit length parameters [18] at the frequency of interest [19]. In this paper calculations were conducted at the dominant frequency $f_{\mathrm{dom}} = 22106$ Hz. Finally, $\mathbf{1}_n$ corresponds to an identity matrix.

To ensure stability, space and time discretization must satisfy the Courant Friedrichs Lewy (CFL) [20] condition:

$$\Delta t \leq \frac{\Delta z}{u} \quad (19)$$

CFL condition suggests that for a stable solution the time step must be no greater than the propagation time along one segment Δz, which for electromagnetic transients on overhead lines is calculated based on the speed of light c [21].

V. Electro-Thermal Coupling

For all GIL segments considered from the VEM analysis, an electrical equivalent circuit, based on the FDTD formulation is considered.

On one hand, in the VEM analysis section, heat generation $\dot{Q}_{\mathrm{g},l}$ representing Joule losses on the conducting layers has been considered. This term contains in practice the coupling, since it is proportional to the square of the conductor current I_k. Therefore, given the conductor resistance R, current at all times for each segment is translated into a heat generation event by (20):

$$\dot{Q}_{\mathrm{g},l} = I_k^2 \cdot R \quad (20)$$

On the other hand, the electrical resistivity of most materials changes with temperature. If the temperature T does not vary significantly, a linear approximation is typically used:

$$\rho(T) = \rho_0[1 + \alpha(T - T_0)] \quad (21)$$

where α is the temperature coefficient of resistivity, T_0 is a reference temperature and ρ_0 is the resistivity at temperature T_0. In this paper, since aluminum is considered, α was taken equal to 0.0039 $^\circ\mathrm{C}^{-1}$.

The above equations represent a bi-directional coupling since current is translated into heat generation, while temperature variations lead to changes on the material resistivity.

VI. Results

A series of scenarios are examined in order to calculate the temperature increase on all layers of the GIL in case of transients. More specifically, lightning surges as well as both single-phase and three-phase short-circuits are examined.

Considering the discretization of the lightning surges, 100 segments are used, i.e. for a total length of 3.3 km dz equals 33 m while dt was taken equal to 0.11 μs. In case of the short circuit scenarios, dz and dt were taken equal to 82.5 m and 0.275 μs, respectively. Finally for the frequency at which calculations are conducted, analysis of [19] has been used.

A. Lightning Surge - Off Load

The lightning surges are simulated by applying a lightning impulse (LI) 1.2/50 μs double-exponential voltage source with an amplitude of 370 kV [22] at the line sending end, whereas no load is connected at the line receiving end. In Figs. 4 and 5, temperature distribution over space and time for the conductor and enclosure are indicated. Although the lightning surge is abrupt and therefore the simulation duration was only 0.1 ms, a marginal temperature increase on both metallic parts is evident. Temperature increase on the inner pipe and on SF_6 layers was even less significant, thus results are not illustrated.

B. Lightning Surge - On Load

The same surge scenario was simulated in case a load equal to 25 Ω was connected at the line receiving end. Temperature on line conducting layers is illustrated in Figs. 6 and 7. Although temperature increase is similar in magnitude with the previous scenario, however due to the load existence the highest temperature increase can be found at the line end rather than at the beginning. Similarly to the previous scenario, inner pipe and SF_6 layers' temperature is not affected at all.

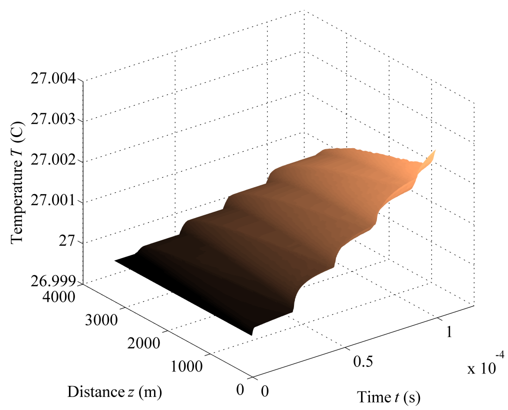

Fig. 4. Conductor temperature for an LI (Off Load).

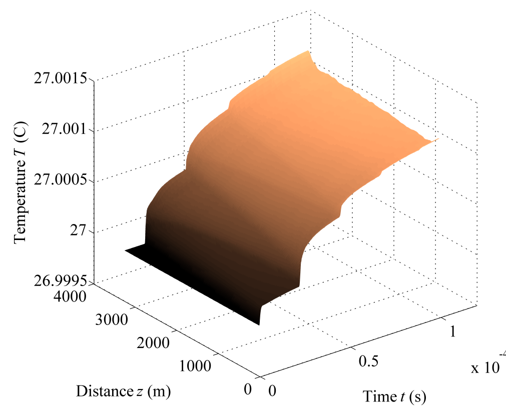

Fig. 6. Conductor temperature for an LI (On Load).

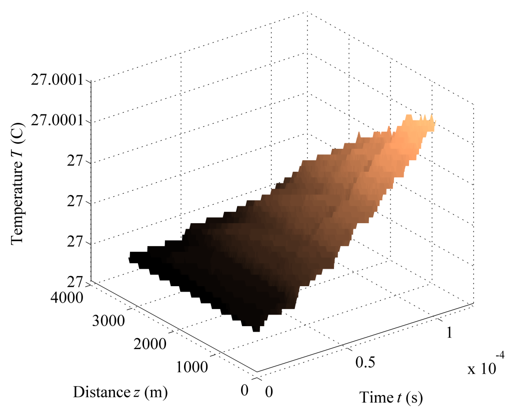

Fig. 5. Enclosure temperature for an LI (Off Load).

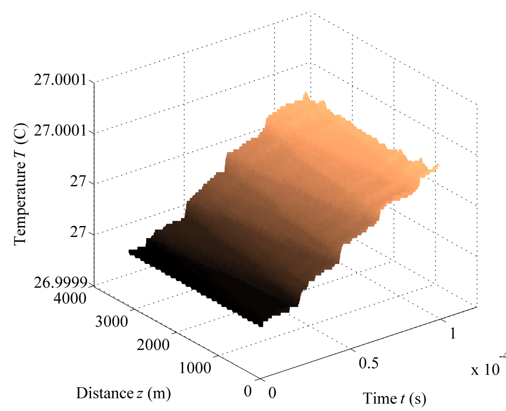

Fig. 7. Enclosure temperature for an LI (On Load).

C. *Single-Phase Short-Circuit*

A single-phase short-circuit is simulated assuming that the receiving end is connected to a load of 25 Ω. The simulation duration is chosen equal to 20 ms in order to capture the influence of slow transients on temperature distribution on all configuration layers. In Fig. 8, temperature distribution over space and time for all layers is illustrated. During the simulation, a rapid temperature increase of more than 150 °C is observed on the conductor, whereas the outer enclosure is also affected by induced currents and indicates an increase of almost 40 °C. As it is evident, in case of a short-circuit, temperature of inner pipe and SF_6 layers is also sightly affected. This transient indicates great impact to all line layer temperature distribution, especially on the metallic parts.

D. *Three-Phase Short-Circuit*

A three-phase short-circuit scenario is also examined. The simulation setup was similar to the previous case. In Fig. 9, the corresponding results are presented. As expected, since this transient is more intense, the conductor temperature is significantly increased, reaching almost 250 °C, i.e. an increase of more than 800%. The outer enclosure temperature is also increased due to induced currents from 27 °C to about 50 °C. Increase on inner pipe and SF_6 layers is less significant.

VII. Conclusions

In this paper, an analytic mathematical formulation regarding electro-thermal modeling of GIL is presented combined with an efficient numerical solution. Simultaneous discretization over space and time based on the FDTD and VEM tools is implemented and combined with an efficient solver to constitute an accurate simulation tool to systematically investigate coupled electro-thermal behavior of GIL lines under transient conditions.

The proposed method is a useful tool to identify a framework, within which operation can be secured without temperature increase to put equipment at risk. Although, steady-state operation scenarios can be modeled, a series of intense transient scenarios are investigated in order to clarify how temperature will be affected under worst-case scenario conditions. The proposed approach can be applied on any configuration given that expressions to describe heat transfer by conduction, convection and radiation have been provided.

Results indicate that the model leads to realistic results, close to those existing in the literature, and that it can be used to analyze the thermal behavior of the GIL for varying time and space under different operating conditions.

Conclusions to the actual design and fabrication of a GIL line are listed as:

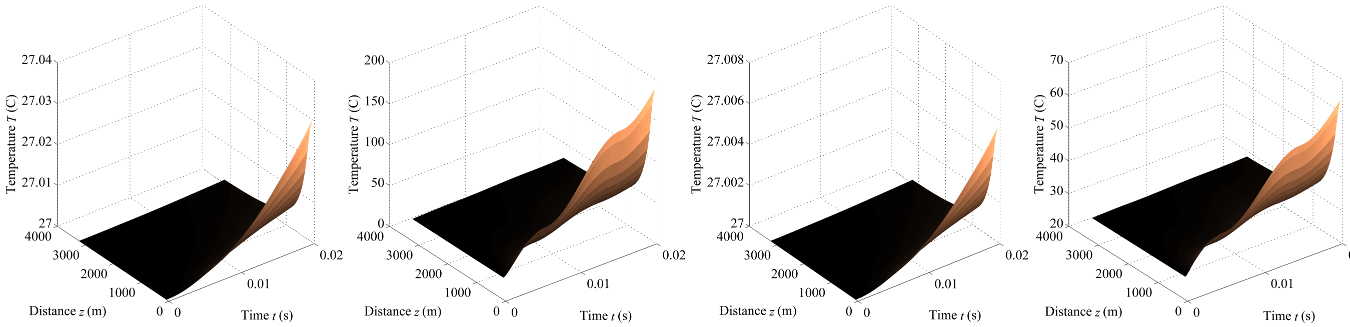

Fig. 8. Temperature distribution for inner pipe, conductor, SF_6 and enclosure layers in case of single-phase short-circuit.

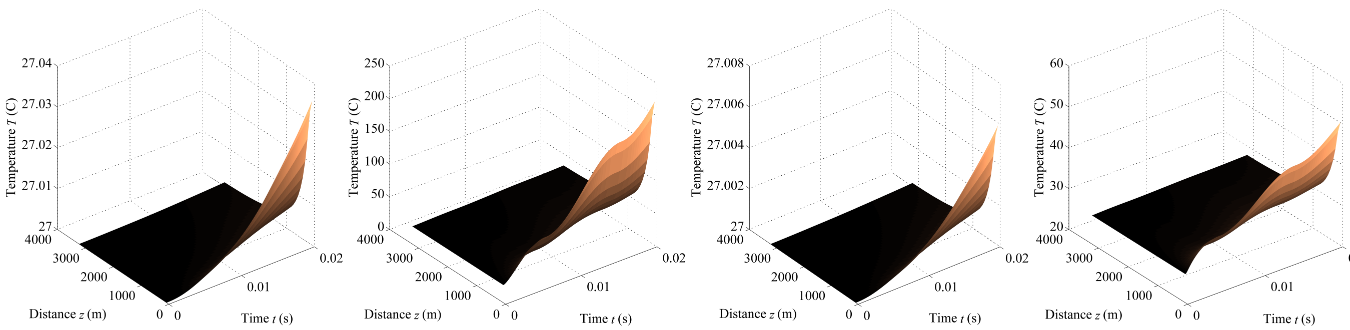

Fig. 9. Temperature distribution for inner pipe, conductor, SF_6 and enclosure layers in case of three-phase short-circuit.

- In case of lightning surges scenarios, temperature increase along the GIL is negligible due to the short duration of the phenomenon.
- For short-circuits, the temperature increase on the conductors is significant and may lead to equipment detoriation if the melting point of Al. (660 °C) is reached.

References

[1] S. Kobayashi, N. Takinami, and A. Miyazaki, "Application of the world's longest gas insulated transmission line (GIL)," in *2003 IEEE Power Engineering Society General Meeting (IEEE Cat. No.03CH37491)*, vol. 4, Jul. 2003, p. 2475 Vol. 4.

[2] T. Nojima, M. Shimizu, T. Araki, and H. Hata, "Installation of a 275 kV-3.3 km gas-insulated transmission line for underground large capacity transmission in Japan," in *International Conference on Large High Voltage Electric Systems, CIGRE*, 1998, pp. 1–3.

[3] H. Koch, "Gas insulated transmission lines - GIL," in *2008 IEEE/PES Transm. and Distrib. Conference and Exposition*, Apr. 2008, pp. 1–3.

[4] R. Benato, C. D. Mario, and H. Koch, "High-capability applications of long gas-insulated lines in structures," *IEEE Trans. Power Del.*, vol. 22, no. 1, pp. 619–626, Jan. 2007.

[5] D. Minaguchi, M. Ginno, K. Itaka, H. Furukawa, K. Ninomiya, and T. Hayashi, "Heat transfer characteristics of gas-insulated transmission lines," *IEEE Trans. Power Del.*, vol. 1, no. 1, pp. 1–9, Jan. 1986.

[6] R. Benato and F. Dughiero, "Solution of coupled electromagnetic and thermal problems in gas-insulated transmission lines," *IEEE Trans. Magn.*, vol. 39, no. 3, pp. 1741–1744, May 2003.

[7] R. Benato, F. Dughiero, M. Forzan, and A. Paolucci, "Proximity effect and magnetic field calculation in GIL and in isolated phase bus ducts," *IEEE Trans. Magn.*, vol. 38, no. 2, pp. 781–784, Mar. 2002.

[8] O. Volcker and H. Koch, "Insulation co-ordination for gas-insulated transmission lines (GIL)," *IEEE Trans. Power Del.*, vol. 16, no. 1, pp. 122–130, Jan. 2001.

[9] A. Miyazaki, N. Takinami, S. Kobayashi, T. Yamauchi, H. Hama, T. Araki, H. Nishima, H. Hata, and H. Yamaguchi, "Line constant measurements and loading current test in long-distance 275 kV GIL," *IEEE Trans. Power Del.*, vol. 16, no. 2, pp. 165–170, Apr. 2001.

[10] D. A. Tsiamitros, T. A. Papadopoulos, and G. K. Papagiannis, "Modeling of gas-insulated lines buried in single and in two-layer earth," in *2009 44th International Universities Power Engineering Conference (UPEC)*, Sep. 2009, pp. 1–5.

[11] R. D. Skeel and M. Berzins, "A method for the spatial discretization of parabolic equations in one space variable," *SIAM J. Sci. Stat. Comp.*, vol. 11, no. 1, pp. 1–32, 1990.

[12] MATLAB, *version 8.2.0.701 (R2013b)*. Natick, Massachusetts: The MathWorks Inc., 2013.

[13] J. A. Souza, J. C. Ordonez, R. Hovsapian, and J. V. C. Vargas, "Thermal modeling of helium cooled high-temperature superconducting DC transmission cable," *IEEE Trans. Appl. Supercond.*, vol. 21, no. 3, pp. 947–952, Jun. 2011.

[14] D. I. Doukas, A. I. Chrysochos, T. A. Papadopoulos, D. P. Labridis, L. Harnefors, and G. Velotto, "Volume element method for thermal analysis of superconducting DC transmission cable," *IEEE Trans. Appl. Supercond.*, vol. PP, no. 99, pp. 1–1, 2017.

[15] IEEE, "IEEE standard of common requirements for high voltage power switchgear rated above 1000 v," *IEEE Std C37.100.1-2007*, 2007.

[16] ——, "IEEE standard for high voltage gas-insulated substations rated above 52 kV," *IEEE Std C37.122-2010*, 2011.

[17] C. R. Paul, *Analysis of multiconductor transmission lines*. John Wiley & Sons, 2008.

[18] F. Rachidi, C. A. Nucci, and M. Ianoz, "Transient analysis of multiconductor lines above a lossy ground," *IEEE Trans. Power Del.*, vol. 14, no. 1, pp. 294–302, Jan. 1999.

[19] A. I. Chrysochos, T. A. Papadopoulos, and G. K. Papagiannis, "Rigorous calculation method for resonance frequencies in transmission line responses," *IET Gener., Transm. Distrib.*, vol. 9, no. 8, pp. 767–778, 2015.

[20] R. Courant, K. Friedrichs, and H. Lewy, "Über die partiellen differenzengleichungen der mathematischen physik," *Mathematische Annalen*, vol. 100, no. 1, pp. 32–74, 1928.

[21] C. G. Kaloudas, A. I. Chrysochos, and G. K. Papagiannis, "FDTD analysis of multiphase power cable systems using distributed constant parameters," in *MedPower 2014*, Nov. 2014, pp. 1–8.

[22] IEC, "Insulation co-ordination - Part 1: Definitions, principles and rules," *IEC 60071-1:2006*, 2006.